Evaluation the Effects of Humidity and Other Process Parameters on TiO$_2$ Nanofibers by RSM (CCD) and Experimental Procedure

Mohammad Hossein Abbaspour-Fard * *and Shadman Mansouri*

Department of Biosystems Engineering, Faculty of Agriculture, Ferdowsi University of Mashhad, Mashhad, Iran

ARTICLE INFO

ABSTRACT

Nanofibers are one of the most widely used materials in various industrial sectors. Among them Titanium Dioxide (TiO$_2$) nanofibers are excelled, moreover they are environmentally friendly and have shown that they have diverse industrial applications. The physical structure of this fiber (diameter and surface characteristics) is a key effective factor on its behavior for corresponding applications. In this study, the effects of different factors influencing the diameter of TiO$_2$ nanofibers were analyzed and quantified using two statistical analyses namely the Response Level Method (RSM) and the Composite Central Design (CCD) method. The preparation parameters of polymer synthesis including the electrical potential, the distance between electrodes tips, flow rate, and ambient humidity were studied. Results marked polymer concentration as the most important factor affecting the diameter of the nanofibers. However the diameter was almost independent from flow rate, and hence marked as the least effective factor. Furthermore, as humidity increased, the diameter of the fibers decreased significantly and surface roughness increased as demonstrated in the SEM and FESEM images. Since the relative humidity has intense impact on the structural properties of titanium dioxide nanofibers, humidity condition of synthesis space must be strictly controlled and kept below a threshold (38%).

INTRODUCTION

One-dimensional (1D) nano-structures such as nanorods, nanowires, and nanotubes and generally the nanocomposites containing various oxide materials have been widely considered by researchers (1) due to their various potential applications. Many applications of different nano-structures can be found in the literature such as solar cells (2, 3), photo-degradation (4, 5) and various other applications (6-9)

Recently, potential applications of titanium Dioxide (TiO$_2$) (including environmental regeneration, electronics, sensors, solar cells, and other related fields) (1-3, 10, 11)motivates researchers. It has been found that surface area property (e.g. large specific surface area) and consequently the mesoporosity of TiO$_2$ improves light absorption. Likewise, the particle dispersion increases the absorbance capacity of the reactants followed by more photocatalytic reactions (12). Therefore, Titanium Dioxide is a broadband semiconductor with many interesting

* Corresponding Author Email: abaspur@um.ac.ir

features such as transparency to transmit visible light, suitable thermal expansion coefficient, and low absorption coefficient. Moreover, it is known as an excellent photocatalyst for degrading organic materials (13). Titanium has two natural polymorphs: rutile and anatase. Generally, only anatase has significant photocatalytic activity (14). Among photocatalyst, anatase phase of TiO$_2$ has been extensively studied. Because this phase of TiO$_2$ has high photocatalytic activity, chemical stability, environmentally friendly and cost-effective (1, 14). Accordingly anatase phase of TiO$_2$ improves stability of the Dye Sensitized Solar Cells (DSSC) (15).

There are several methods to synthesize TiO$_2$ nanofibers, such as sol-gel, electrospinning, etc. Among these, electrospinning is an excellent method for producing synthetic fibers like carbon, organic and inorganic hybrid nanowires and other fibers in nanoscale (16) due to low price, variability, and simple process (17).

The electrospinning process involves a high voltage source connected to a needle and a metal collector, where the fibers are accumulated (18). The needle is attached to an injection pump, where a polymeric solution is delivered. The needle is connected to the positive electrode and the collector is connected to the negative electrode. As a result, a difference in potential between the collector and the needle of the electric field is generated which causes drops on the needle to be drawn and nanofibers is formed (19). When the applied electric field overcomes the surface tension of a droplet, the solution is drawn, heading to the negative electrode as a jet to form fibers on the surface of the collector (20). As these fibers are in nanoscale, they have a very large surface-to-volume ratio. The diameter and morphology of the fibers can be adjusted by changing the rheological properties of the solution and the process parameters of the electrospinning (18).

The results of research studies on fibers synthesized by electrospinning indicate that several factors such as solubility, tip-collector distance, temperature, humidity, etc. affect their structure and morphological properties. Most electrospinning processes are generally performed in an uncontrolled environmental condition with unknown and variable relative humidity. However, to understand the formation of fibers under varying relative humidity conditions, limited

number of studies have been carried out (21, 22).

Several published works on synthesis of titanium dioxide nanofibers are appeared in the literature, to study the effect of three key parameters (injection rate (mL/h), potential difference (kV), and synthesis solution concentration) on fiber diameter (18, 23). In some reports, the so-called Response Level Method (RSM) as statistic model has been used to predict the diameter of titanium dioxide in the electrospinning process. In a study conducted by Li and Xia (2003), three electrospinning parameters including the voltage between tip and collector and tip-collector distance (TCD, the distance between the positive and negative electrodes) were investigated by the Box-Behnken Design (BDD) method during synthesis of nanofibers (23). In another study, six effective parameters (TCD, voltage, flow rate, amount of PVC, amount of TTIP and pH) were studied using two statistical analyses, Response Level Method (RSM) and Box–Wilson central composite design (CCD) techniques (24). The RSM is a statistical method for analyzing the effects of several independent variables for the response. This method uses multivariable data in experiments that are designed to solve multivariate equations simultaneously (25). Additionally, the main advantage of RSM is to reduce the number of empirical experiments needed to evaluate different variables and their interactions. Therefore, RSM makes simplicity and reduces the time and cost more than that of classical methods spend to optimize a process (26). There was neither enough number of effective electrospinning parameters nor statistical validity to support results out of previous studies on nanofibers fabricated from TiO$_2$

In the current study, the synthesized TiO$_2$ nanofibers were characterized and analyzed under various processing conditions each in five levels. These parameters were flow rate of the synthesis solution from 0.1 to 0.9 mL/h, the voltage between the needle tip and the collector ranged from10 to 30 kV, the distance between the needle tip and the collector (TCD) ranged from10 to 30 cm, the percent of PVP in the polymeric solution (5 to 13%) and the ambient relative humidity under controlled conditions at five levels (ranged from 24 to 42 %).

By comparing the methodology of the current research with those of previous research works, its novelty is well appeared. While in a previous
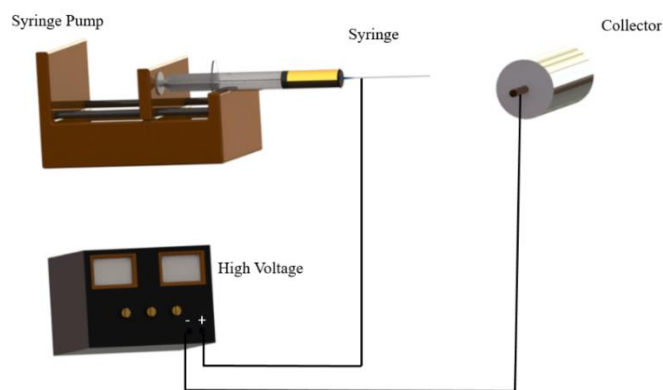
Fig. 1. A typical electrospinning setup

work (27) sampling was completely random, in the current research all parameters are designed and optimized using the Design Expert software, Response Surface Model (RSM) and Composite Central Design (CCD). Hence, the synthesis process is performed accurately, but at a lower cost and reproducibility is also improved. The outputs of the software are three-dimensional diagrams representing the effect of each parameter on diameter of the synthesized nanofibers were investigated. Moreover, in the previous studies the parameters were mostly investigated individually, but in the current study all of the parameters are examined in an integrated manner with more emphasis on humidity of the synthesizing space. Therefore, the current study has the excellence and innovation in examining titanium dioxide nanofibers as it shows the following attributes: 1) High test accuracy (low error), 2) Examine the process parameters at acceptable levels and 3) The study explored the impact of ambient relative humidity as a significant parameter on diameter of the synthesized nanofibers for the first time and with great accuracy of morphology and diameter.

MATERIAL AND METHODS
Solution preparation

In order to synthesis TiO₂ nanofibers by electrospinning technique, PVP (Mw 1,300,000 g mol⁻¹ and TTIP (Ti(OiPr)$_4$, both from Aldrich) were used as precursor materials. The preparation procedure of electrospinning solutions was performed in three steps. In the first step 2 mL of TIPP, 2 mL of absolute ethanol and 2 mL of glacial acetic acid were mixed for about 10 min. In the second step 0.1, 0.3, 0.5, 0.7 and 0.9 mL

of PVP and 6 mL of absolute ethanol were mixed separately for about 10 min. In the last step, the solution containing the TTIP was added to the polymer solution dropwise and stirred for about 30 min. Finally, to make a viscous electrospinning solution, it was heated at 50 ºC for about 10 min.

Electrospinning

In the electrospinning process, the PVP/TIPP solution was loaded in a syringe with a 21 gauge stainless steel needle. The syringe was placed in the syringe pump and the flow rate levels were set as 0.1, 0.3, 0.5, 0.7 and 0.9 mL/h. The distance between the needle tip and collector was altered from 10 to 30 cm. To collect the synthesized nanofibers easily, the surface of collector was covered with an aluminum foil. One of the key parameters in electrospinning process is the voltage between the needle tip and collector (10) that was set between 10-30 kV. A typical electrospinning setup system is shown in Fig. 1. Each experimental run of the synthesizing nanofibers samples (Fig. 2) lasted for about 20 min.

The collected nanofibers were kept in laboratory for about two hours to remove moisture and then calcinated at 300, 400 and 500 ºC. During the calcination procedure, the diameter of the fibers was decreased as organic components such as PVP were burnt out. Therefore, calcination formed and changed the phase of fiber from anatase to rutile.

To control the relative humidity of the synthesizing space and provide various levels of this parameter, a closed chamber made of glass and a steam generator were provided to isolate the electrospinning space. The ambient relative
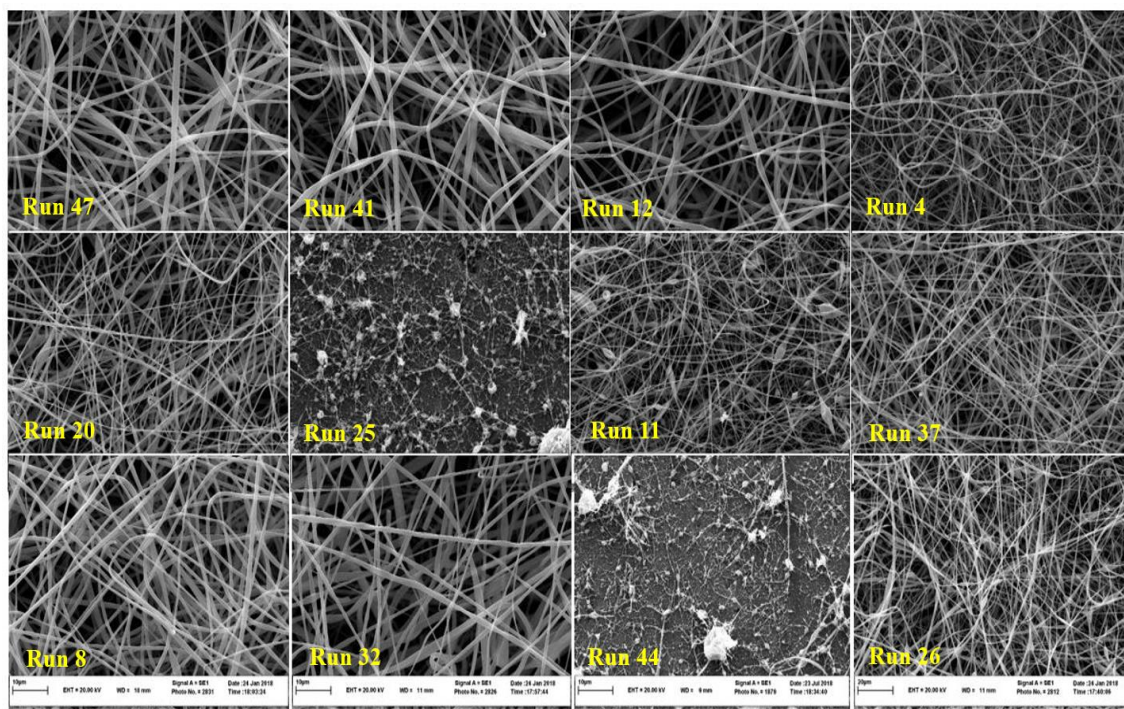
Fig. 2. Examples of nanofibers synthesized under various process parameters. It is seen that the TiO$_2$ nanofibers diameter is obviously altered as the process parameters are changed.

humidity was set at five levels as 24, 28.5, 33, 37.5 and 42 %. The synthesized nanofibers can be used in many applications such as solar cells and photocatalyst activity.

Nanofiber Characterization

The diameter and morphology of the electrospun TiO$_2$ nanofibers were investigated by Scanning Emission Microscope (SEM) (Leo 1450VP, Germany) and Field Emission Scanning Electron Microscope (FESEM) (MIRA3 TE SCAN, Czech Republic). Morphological and structural analysis were studied by Transmission Electron Microscope (TEM) (Leo 912 AB, Germany). Crystallization measurements were performed by X-Ray Diffraction (XRD) (EXPLORER, Italy) with CuKα line, from 20 to 80°. FTIR (AVATAR 370 FT-IR, USA) was used to find out the functional groups of the TiO$_2$ nanostructures.

Experimental Design

Using the Design Expert software version 10, a five-factor, five-level Central Composite Design (CCD) was established to verify the impact of process variables, namely PVP concentration (X_1), voltage (X_2), distance (X_3), humidity (X_4), and flow rate (X_5) on diameter of the TiO$_2$ nanofibers. Screening experiments were carried out to determine the range of variables. The parameters and their levels are shown in (Table 1). A total of 50 experimental runs were performed in triplicate, including 8 replicates of the center point for each variable.

Statistical analysis

In order to obtain the empirical models that predict the response, different regressions were fitted to the data. These models were statistically compared to select the appropriate model. It is noteworthy to say that a statistical model is suitable when "lack of fit" is not significant and it has the highest R^2, "R^2 adjusted" and "R^2 predicted". To select the appropriate model for predicting the desired response, the lack of fit test was performed. The significance of a lack of fit test for a model indicates that the model does not have the ability to predict the results for new observations. Therefore, the insignificance of the lack of fit test means that the model is able to be fit well with the empirical data. The "*F*" test was also performed to compare and analyze the variance (ANOVA) of the models and parameters.

Table 1. Variables and their corresponding levels for the CCD

Factor	Symbol	Coded Factor				
		-2	-1	0	-1	2+
PVP (%)	X$_1$	5	7	9	11	13
Voltage (kV)	X$_2$	10	15	20	25	30
Distance (cm)	X$_3$	10	15	20	25	30
Humidity (%)	X$_4$	24	28.5	33	37.5	42
Flow Rate (mL/h)	X$_5$	0.1	0.3	0.5	0.7	0.9

The analysis of variance was applied for the response. The model has been statistically significant about the response (P < 0.05). To show the significance of the variables on the response, "F- test" and (p< 0.05) were used. Non-significant variables were eliminated by the backward elimination algorithm, which reduced the number of terms in the polynomial models. The results of statistical analysis of the fitted model show that this model has optimum response to a high-performance and high-power response considering R^2, R^2 adjusted and R^2 predicted. All experiments were carried out randomly in triplicate.

The effect of independent variables on the response

In RSM, for each dependent variable there is a model that expresses the principal and reciprocal effects of factors on each separate variable. The multivariate model is written as:

$$Y = \beta_0 + \beta_1X_1 + \beta_2X_2 + \beta_3X_3 + \beta_4X_4 + \beta_5X_5 + \beta_{12}X_1X_2 + \beta_{13}X_1X_3 + \beta_{14}X_1X_4 + \beta_{15}X_1X_5 + \beta_{23}X_2X_3 + \beta_{24}X_2X_4 + \beta_{25}X_2X_5 + \beta_{34}X_3X_4 + \beta_{35}X_3X_5 + \beta_{45}X_4X_5 + \beta_{11}X_1^2 + \beta_{22}X_2^2 + \beta_{33}X_3^2 + \beta_{44}X_4^2 + \beta_{55}X_5^2 \tag{1}$$

where, Y is the predicted response (diameter of nanofibers), X$_1$, X$_2$, X$_3$, X$_4$ and X$_5$ are the affecting parameters, β_0 is the interception coefficient, β_1, β_2, β_3, β_4 and β_5 are constant coefficients. In other words, this equation expresses the relation between TiO$_2$ nanofibers' diameter and all the affecting parameters taken into account in the current study.

Response surface

Surface plots provide the relationship between responses and the experimental levels of each parameter (variable), as well as the type of interactions between two test variables, and hence determine the optimal level of each factor. In each plot, the response surface level was plotted using the Design Expert software version 10. Moreover, empirical data were optimized, the experimental factors were examined in triplicate and theoretical and actual values were compared. Eventually, the effect of humidity of synthesis environment on TiO$_2$ nanofibers were investigated. In this section the main objective was to study the variation of diameter and morphology of nanofibers under varying ambient humidity.

RESULT AND DISCUSSION

As previously mentioned Design Expert software used and a five-factor, five-level Central Composite Design (CCD) was established to verify the impact of process variables, namely concentration (X$_1$), voltage (X$_2$), distance (X$_3$), humidity (X$_4$), and flow rate (X$_5$) on the diameter of TiO$_2$ nanofibers. The CCD matrix of the predicted and observed results of the electrospinning of TiO$_2$ nanofibers are presented in Table 2.

In order to obtain a suitable experimental model for predicting the response of Nanofibers diameter, various regressions were fitted to the data. These models were then analyzed to select the appropriate model. As illustrated in Table 3, the best model to predict the responses was quadratic model.

From statistical point of view, a desired model is the one in which the goodness of fit test (p (lack of fit) > 0.05) is not significant, and also has the highest value of R^2 *adjusted* and R^2 *predicted*. The details of statistical analysis of the models fitting for responses are presented in (Table 4). According to this Table, the goodness of fit test of the fitted model on the responses was not significant. Therefore, the selected model and the test have a very high degree of certainty.

According to the ANOVA analysis for the responses (see Table 3 and Table 4), the quadratic model did not agree with the statistical tests reference values. It is noteworthy that after fitting, the model was subjected to an algorithm that eliminates feedbacks and hence the number

Table 2. CCD matrix, experimental and predicted values for the response variables

											Response	
	Coded Levels					Independent variable					Actual	Predicted
Run	X$_1$	X$_2$	X$_3$	X$_4$	X$_5$	PVP (%)	Voltage (kV)	Distance (cm)	Moisture (%)	Flow Rate (mL/h)	Diameter (nm)	Diameter (nm)
1[1]	-1.000	-1.000	1.000	1.000	1.000	7	15	25	37.5	0.7	0	-
2	-1.000	1.000	1.000	-1.000	-1.000	7	25	25	28.5	0.3	18	70.84
3	-1.000	-1.000	1.000	-1.000	-1.000	7	15	25	28.5	0.3	33	103.83
4	-1.000	-1.000	-1.000	-1.000	1.000	7	15	15	28.5	0.7	822	966.09
5	1.000	1.000	-1.000	-1.000	-1.000	11	25	15	28.5	0.3	436	591.73
6[a]	-1.000	-1.000	1.000	1.000	-1.000	7	15	25	37.5	0.3	0	-
7[b]	0.000	0.000	0.000	0.000	0.000	9	20	20	33	0.5	412	324.14
8	0.000	0.000	0.000	-2.000	0.000	9	20	20	24	0.5	952	1096.08
9	-1.000	1.000	-1.000	-1.000	1.000	7	25	15	28.5	0.7	513	423.25
10	1.000	1.000	1.000	-1.000	-1.000	11	25	25	28.5	0.3	407	282.61
11	-1.000	1.000	1.000	1.000	-1.000	7	25	25	37.5	0.3	286	374.48
12	1.000	-1.000	1.000	-1.000	-1.000	11	15	25	28.5	0.3	1112	1169.94
13	-1.000	1.000	-1.000	1.000	1.000	7	25	15	37.5	0.7	59	72.24
14[2]	0.000	0.000	0.000	0.000	0.000	9	20	20	33	0.5	278	324.14
15	0.000	-2.000	0.000	0.000	0.000	9	10	20	33	0.5	902	952.59
16	0.000	0.000	0.000	0.000	-2.000	9	20	20	33	0.1	269	212.54
17	0.000	0.000	0.000	0.000	2.000	9	20	20	33	0.9	712	831.30
18	0.000	2.000	0.000	0.000	0.000	9	30	20	33	0.5	119	131.26
19[b]	0.000	0.000	0.000	0.000	0.000	9	20	20	33	0.5	242	324.14
20	1.000	1.000	-1.000	1.000	1.000	11	25	15	37.5	0.7	778	726.56
21	-1.000	-1.000	-1.000	1.000	1.000	7	15	15	37.5	0.7	67	6.24
22[b]	0.000	0.000	0.000	0.000	0.000	9	20	20	33	0.5	284	324.14
23	-1.000	1.000	-1.000	-1.000	-1.000	7	25	15	28.5	0.3	233	156.35
24	1.000	1.000	1.000	1.000	1.000	11	25	25	37.5	0.7	248	318.50
25[a]	-2.000	0.000	0.000	0.000	0.000	5	20	20	33	0.5	0	-
26	1.000	1.000	-1.000	1.000	-1.000	11	25	15	37.5	0.3	425	323.16
27[b]	0.000	0.000	0.000	0.000	0.000	9	20	20	33	0.5	396	324.14
28	1.000	-1.000	-1.000	1.000	-1.000	11	15	15	37.5	0.3	872	985.99
29	-1.000	-1.000	-1.000	-1.000	-1.000	7	15	15	28.5	0.3	693	573.68
30	-1.000	-1.000	-1.000	1.000	-1.000	7	15	15	37.5	0.3	196	190.38
31	1.000	-1.000	-1.000	-1.000	-1.000	11	15	15	28.5	0.3	1968	1863.40
32	1.000	-1.000	-1.000	1.000	1.000	11	15	15	37.5	0.7	1536	1514.90
33	1.000	-1.000	1.000	1.000	-1.000	11	15	25	37.5	0.3	378	370.64
34	-1.000	1.000	1.000	-1.000	1.000	7	25	25	28.5	0.7	207	160.69
35[b]	0.000	0.000	0.000	0.000	0.000	9	20	20	33	0.5	413	324.14
36[b]	0.000	0.000	0.000	0.000	0.000	9	20	20	33	0.5	367	324.14
37	-1.000	1.000	-1.000	1.000	-1.000	7	25	15	37.5	0.3	336	381.89
38	0.000	0.000	2.000	0.000	0.000	9	20	30	33	0.5	293	206.97
39	0.000	0.000	0.000	2.000	0.000	9	20	20	42	0.5	27	-54.23
40	-1.000	-1.000	1.000	-1.000	1.000	7	15	25	28.5	0.7	399	319.19
41	1.000	-1.000	1.000	-1.000	1.000	11	15	25	28.5	0.7	2116	2098.35
42	1.000	-1.000	-1.000	-1.000	1.000	11	15	15	28.5	0.7	3115	2968.86
43	1.000	1.000	1.000	-1.000	1.000	11	25	25	28.5	0.7	1057	1085.51
44[a]	-1.000	1.000	1.000	1.000	1.000	7	25	25	37.5	0.7	0	-
45	1.000	1.000	1.000	1.000	-1.000	11	25	25	37.5	0.3	88	92.15
46	1.000	-1.000	1.000	1.000	1.000	11	15	25	37.5	0.7	711	722.50
47	1.000	1.000	-1.000	-1.000	1.000	11	25	15	28.5	0.7	1628	1571.68
48	0.000	0.000	-2.000	0.000	0.000	9	20	10	33	0.5	936	1084.88
49	2.000	0.000	0.000	0.000	0.000	13	20	20	33	0.5	1342	1404.85
50[b]	0.000	0.000	0.000	0.000	0.000	9	20	20	33	0.5	264	324.14

[a] The fibers are not formed

[b] Center Point

Table 3. Validation of the proposed regression models

Source	Sequential p-value	Lack of Fit p-value	Adjusted R^2	Predicted R^2	Remark`
Linear	< 0.0001	< 0.0001	0.6636	0.5824	
2FI	< 0.0001	0.0076	0.9296	0.8953	
Quadratic	< 0.0001	0.0767	0.9687	0.9257	Suggested
Cubic	0.0533	0.2962	0.9849		Aliased

Table 4. ANOVA for Response Surface Quadratic model

Source	Sum of Squares	df	Mean Square	F Value	p-value Prob > F	
Model	1.739E+007	18	9.661E+005	75.09	< 0.0001	significant
X_1-PVP	4.897E+006	1	4.897E+006	380.63	< 0.0001	
X_2-Voltage	1.440E+006	1	1.440E+006	111.92	< 0.0001	
X_3-Distance	1.650E+006	1	1.650E+006	128.21	< 0.0001	
X_4-Moisture	2.817E+006	1	2.817E+006	218.92	< 0.0001	
X_5-Flow Rate	8.113E+005	1	8.113E+005	63.06	< 0.0001	
X_1X_2	1.268E+006	1	1.268E+006	98.53	< 0.0001	
X_1X_3	71512.29	1	71512.29	5.56	0.0259	
X_1X_4	3.726E+005	1	3.726E+005	28.96	< 0.0001	
X_1X_5	8.876E+005	1	8.876E+005	68.99	< 0.0001	
X_2X_3	2.648E+005	1	2.648E+005	20.58	0.0001	
X_2X_4	6.505E+005	1	6.505E+005	50.56	< 0.0001	
X_3X_5	59985.70	1	59985.70	4.66	0.0399	
X_4X_5	5.846E+005	1	5.846E+005	45.43	< 0.0001	
X_1^2	50648.72	1	50648.72	3.94	0.0575	
X_2^2	90032.78	1	90032.78	7.00	0.0134	
X_3^2	1.972E+005	1	1.972E+005	15.33	0.0006	
X_4^2	73430.06	1	73430.06	5.71	0.0241	
X_5^2	74182.33	1	74182.33	5.77	0.0235	
Residual	3.474E+005	27	12866.00			
Lack of Fit	3.112E+005	20	15557.80	3.01	0.0704	not significant
Pure Error	36226.00	7	5175.14			
Cor Total	1.774E+007	45				

of model parameters was decreased. Also, the fitness test for the responses was not significant. The significance of values of the test show that the studied model does not have the ability to predict the values of the function. In other words, the significance of the test does not mean that the model is able to be fit well in accordance to the test data. Based on the results presented inTable 3, in terms of statistical analysis of the fitted model, high-power and high-performance coefficients (R^2, R^2 Adjusted and R^2 Predicted) for optimization are met.

As previously stated (Eq.1), RSM scheme is defined for each independent variable of the model indicating main and mutually exclusive effects of parameters for each variable. According to the analysis of variance (Table 4), it was determined that the main effects (X_1, X_2, X_3, X_4, X_5) and interactions (X_1X_2, X_1X_4, X_1X_5, X_2X_3, X_2X_4, X_4X_5) and quadratic effect (X_3^2) on nanofiber diameter response were significant at the 99% (P < 0.0001) confidence level. Similarly, the effect of X_1X_3, X_3X_5, X_2^2, X_4^2 and X_5^2 was significant at 95% level (P < 0.05). However, other parameters did not have notable effect on response (diameter) at 95% level. The highest mean diameter was related to

the sample 42 (3115 nm) and lowest value was recorded for the sample 2 (18 nm). Eventually, the predicting relationship was provided as follows:

Y (Diameter) = +324.14 + 430.11 X$_1$ - 205.33 X$_2$ - 219.48 X$_3$ - 287.58 X$_4$ + 154.69 X$_5$ - 213.58 X$_1$X$_2$ - 55.90 X$_1$X$_3$ - 123.53 X$_1$X$_4$ + 178.26 X$_1$X$_5$ + 96.08 X$_2$X$_3$ + 152.21 X$_2$X$_4$ - 31.38 X$_2$X$_5$ +19.53 X$_3$X$_4$ - 44.26 X$_3$X$_5$ - 144.14 X$_4$X$_5$ + 55.12 X$_1^2$ + 54.44 X$_2^2$ + 80.44 X$_3^2$ + 49.19 X$_4^2$ +49.44 X$_5^2$ (2)

The surface plots of representing interaction effects of the independent variables are depicted in Fig. 3a, the effect of polymer content (ranged from 7 to 11 percent), on nanofibers' diameter, is very clear, however the effect of voltage (from 15 to 25 kilovolts), on diameter reduction is very low and not impressive. In general, the interaction of these two variables increases the diameter of nanofibers. Hence, it can be concluded that with a constant voltage, increasing the concentration of polymer, significantly increases the diameter of nanofibers, which agrees with a study led by Mali et al. (2015). They conducted similar study on polymer concentration for nanofiber synthesis. In this experiment, they concluded that the more polymer concentration, the bigger diameter of fibers (18).

According to the plot of Fig. 3b, the two factors of polymer content and distance of electrodes have different effects on the diameter of nanofibers. With decrease of electrodes distance and increase of polymer content, the fiber diameter grows. In other words, with a constant distance, with increase of polymer concentration, nanofiber diameter also increases. In contrast, with a constant polymer concentration, with increasing electrode distance, the diameter of the Nanofibers decreases. However, according to the interaction graph (Fig. 3b), the interaction of these two factors has an increasing effect on diameter of nanofibers. This is mainly due to the much greater impact of polymer concentration on the diameter of the nanofibers than the electrode distance. This finding is in agreement with Sarlak et al. (24) who stated that increasing polymer concentration had the greatest effect on the electrospun nanofiber diameter.

Increasing the relative humidity of the synthesis environment noticeably decreases the diameter of nanofibers which is seen in Fig. 3c. A fairly linear reduction in diameter is seen when relative humidity increases from 24 to 37.5 percent. In general, the interaction of polymer concentration and humidity increases the diameter of the nanofibers, marking greater effect of polymer concentration on the fiber diameter than the effect of relative humidity. The Injection rate of synthesis solution assessment indicates that an increase in flow rate led to an increase in diameter of the nanofibers (Fig. 3d). However considering the detailed data it is seen that, this parameter has the least effect on diameter of the nanofibers.

According to Fig. 3e an instantaneous reduction in voltage and electrode distance increases the diameter of nanofibers, however, the effect of the former is less important than the latter. Hence, the interaction effect of these two parameters also increases the diameter of nanofibers. Comparing the graphs of Fig. 3b and Fig. 3e it can be seen that the effects of these two factors are fairly less than the effect of polymer concentration on the diameter of nanofibers. Considering the effect of voltage and the relative humidity of environment (Fig. 3f), it is evident that both parameters reduce the diameter of nanofibers, nonetheless, the effect of humidity is greater than the voltage. In other words, the effect of relative humidity on reduction of nanofibers' diameter is more noticeable than the voltage. Fig. 3g shows that the effect of increasing flow rate on the increase in diameter of nanofibers is in contrast to the effect of increasing voltage. However, the nanofibers' diameter is more affected by voltage variation than flow rate Based on the diagram of Fig. 3h, the interaction between the electrode distance and the relative humidity of environment has an increasing effect on the diameter of nanofibers with their increase. However, the relative humidity is fairly more effective than the distance of electrodes. The effect of increasing electrodes distance on reduction of nanofibers diameter is somehow higher than the decrease of flow rate (Fig. 3i), therefor their interaction decreases the diameter of nanofibers. It is also seen that the increase of humidity and decrease of flow rate have a decreasing effect on the diameter of nanofibers (Fig. 3j). But the effect of the humidity of laboratory space (synthesis environment) is far greater than the flow rate.

This can be implied from the inclination of the graph i.e. the humidity has a steeper slope than the other. It can be concluded that the relative humidity of the space of nanofiber synthesis laboratory is a key parameter affecting the
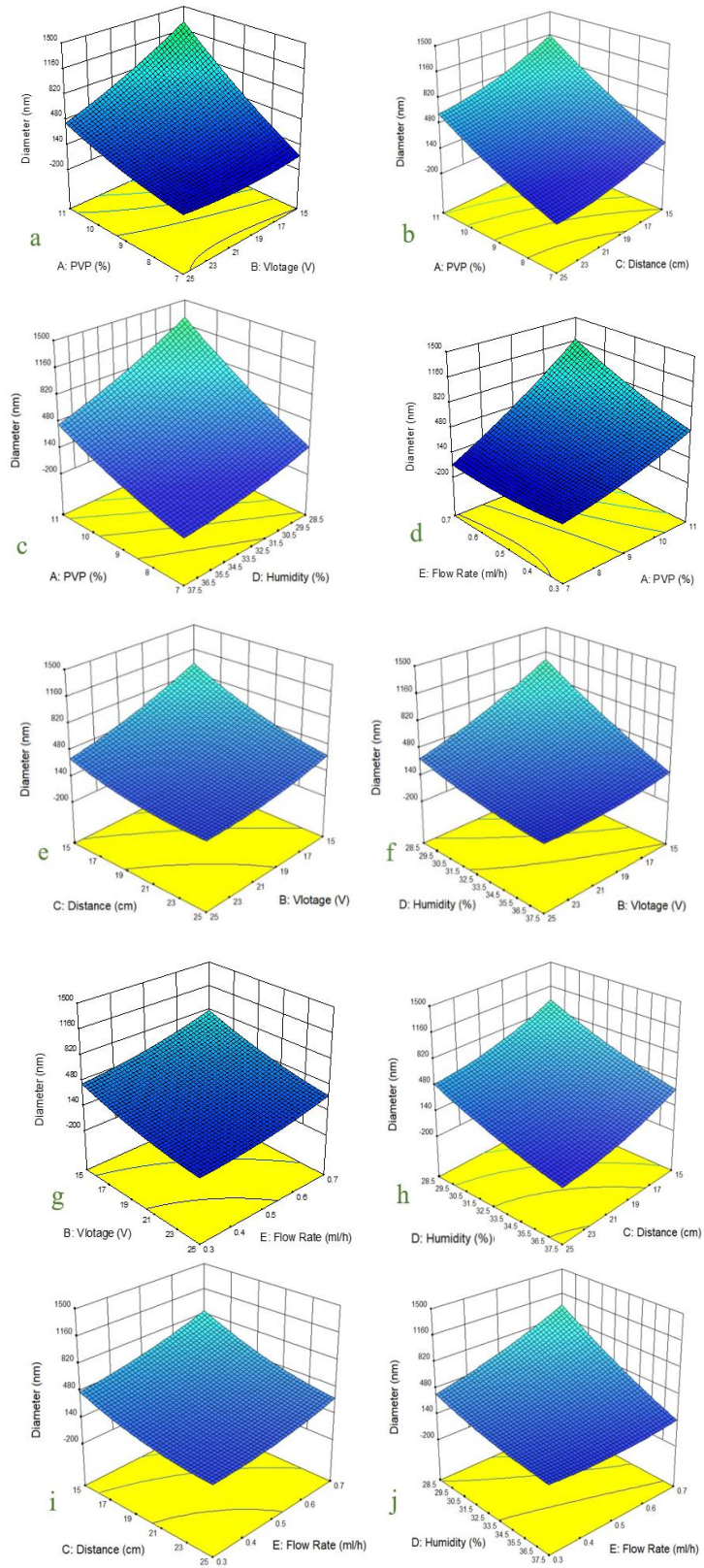
Fig. 3. Surface plots for the interaction effects of independent variables on diameter

Table 5. Prerequisites of the electrospinning process optimization

Name	Goal	Lower Limit	Upper Limit	Lower Weight	Upper Weight	Importance
X_1:PVP	Is in range	7	11	1	1	3
X_2:Voltage	Is in range	15	25	1	1	3
X_3:Distance	Is in range	15	25	1	1	3
X_4:Moisture	Is in range	28.5	37.5	1	1	3
X_5:Flow Rate	Is in range	0.3	0.7	1	1	3
Diameter	Is in range	100	200	1	1	3

Table 6. Predicted and experimental results of the electrospinning process optimization

PVP	Voltage (kV)	Distance (nm)	Moisture (RH %)	Flow Rate (mL/h)	Predicted Diameter (nm)	Desirability	Actual Diameter (nm)	Actual Diameter (nm)
8.850	17.097	21.282	36.879	0.659	131.263	1.000	86 ± 3	113 ± 5

geometrical properties of the nanofibers (more specifically their diameter) which should be controlled during nanofibers synthesis.

Optimization procedure

The effect of five process parameters namely voltage between electrodes, needle tip-electrode distance, injection rate (flow rate), concentration of synthesis solution (polymer content) and relative humidity of synthesis space (laboratory) on the diameter of titanium dioxide nanofibers were investigated, in five levels using the RSM method. These results are presented in Table 5 and Table 6.

According to Table 5, the high and low values of the effective factors on the response are in particular suffered to examine the correctness of the optimization and the success of the model. As it is seen the optimization should be achieved with a polymer content of 8.850 %, a voltage of 17.097 kV, an electrodes distance of 21.282 nm, a relative humidity of 36.879 %, and an injection rate of 0.659 mL/h in a test of 131.26 nm in diameter, which is predicted by the software. Accordingly, experiments were performed experimentally with the software prognostic standard, with a diameter of 113 nm, which is very close to the predicted value. The confidence interval and predication interval were used to prove this and the appropriateness of the experimental value. Based on the 95% confidence that the software is predicting**,** if the values obtained are empirically between 109.824 and 120.126 (confidence interval) and between 129.72 and 137.270

(Prediction interval), it can be claimed that the model in prediction was successful. This is quite true given the range and the experimental value obtained. Therefore, it can be safely said that a successful model, using the conditions in each experiment, can be approached similarly.

Characterization of titanium dioxide nanofibers

As stated previously, different process parameters have different impact on the diameter and morphology of the nanofibers. In this section, a statistical method is employed to predict the diameter of the fibers under different relative humidity and examine the effect of relevant parameters. It is noteworthy that relative humidity of synthesis environment by electrospinning method has not yet been considered as a key variable in such a process. In this part of the current study this parameter was thoroughly examined by considering five different levels (24, 28.5, 33, 37.5 and 42%) and the results revealed an interesting trend. The TiO₂ nanofibers were synthesized by electrospinning method with constant parameters including voltage (20 kV), polymer content (5.0 g per 5 mL absolute ethanol), titanium isopropoxide (1 mL titanium isopropoxide in 4 mL solution with 1:1 absolute ethanol and Glacial acetic acid), the flow rate (0.3 mL/h) and the distance between the electrodes (15 cm).

To remove the impurities, the synthesized nanofibers were then heated at 530 °C. This thermal treatment also created a crystal structure in the nanofibers. The morphological characteristics of the Nanofibers were then analyzed by FESEM,
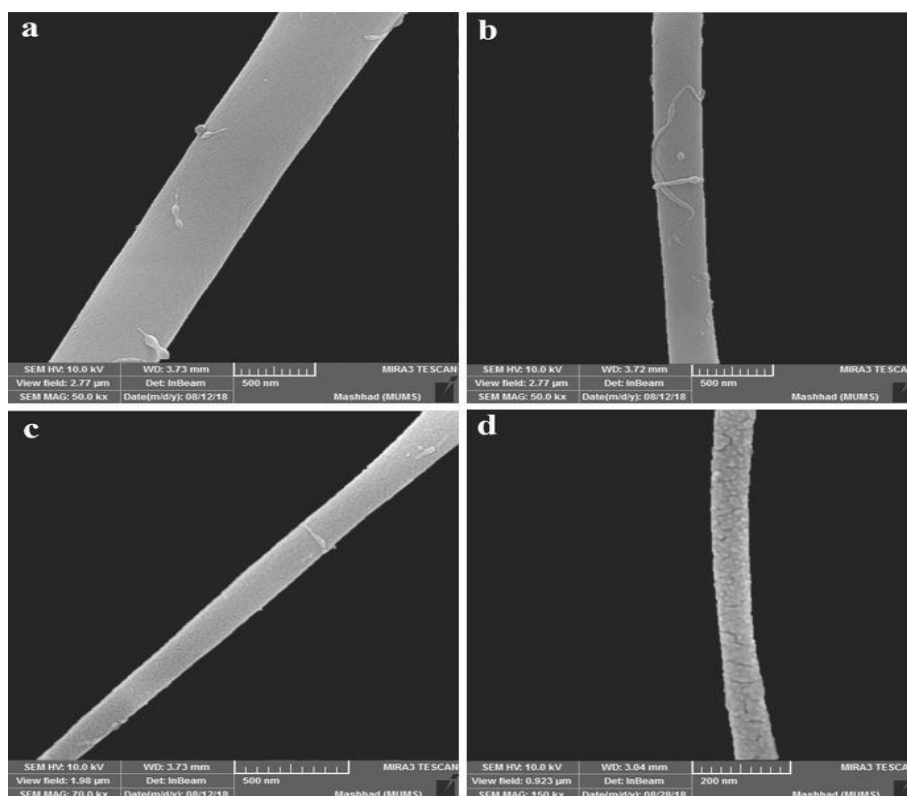
Fig. 4. FESEM image of the formation of synthesized TiO$_2$ nanofibers at various ambient relative humidity: a) R.H 24%; D= 525 nm b) R.H 28.5%; D= 308 nm, c) R.H 33%; D= 166 nm and d) R.H 37.5%; D= 67 nm

SEM, TEM, XRD, and FTIR.

The SEM and FESEM analyses were used to investigate the appearance of the nanofibers, including diameter and morphology. The diameter and morphology of the electrospun nanofibers are shown in Fig. 4 and Fig. 5 obtained from a sol-gel polymer solution (2 mL TIPP, 2 mL absolute ethanol and 2 mL acetic acid glacial in titanium solution and 0.3 PVP content in the polymer solution). The fibers were subjected to calcination at 530 °C using SEM and FESEM analyses. In the SEM images, four photos of the nanofibers (Fig. 4 and Fig. 5) were provided at a voltage of 20 kV, flow rate of 0.3 mL/h, electrodes distance of 20 cm, and constant concentration with a polymer content of 9% while the relative humidity varied from 24% to 42%. According to Fig. 4a, it is observed that the nanofibers with the lowest ambient humidity of 24%, have diameter of 525 nm and low morphology (exhibiting some additional outgrowth appendages on the surface). At relative humidity of 28.5%, the diameter reduced to 308 nm and their morphology was also improved.
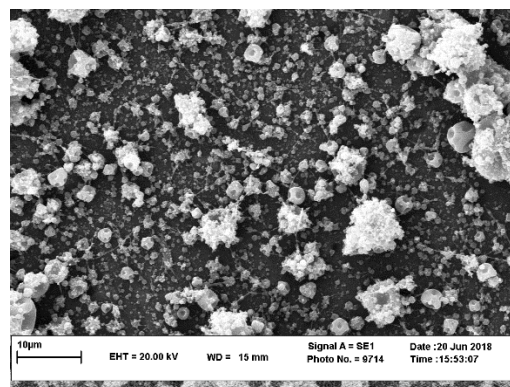

Fig. 5. SEM image of the "unformed" TiO$_2$ Nanofibers at a high ambient relative humidity (42 %)

Further reductions in diameter and improvements in morphology are seen (166 nanometer at 33%, and 67 nm at 37.5%) as the ambient humidity increased. However, when ambient humidity rose to 42%, the nanofibers failed to form and hence sprayed onto the aluminum foil in form of some amorphous spots (Fig. 5). In other words,
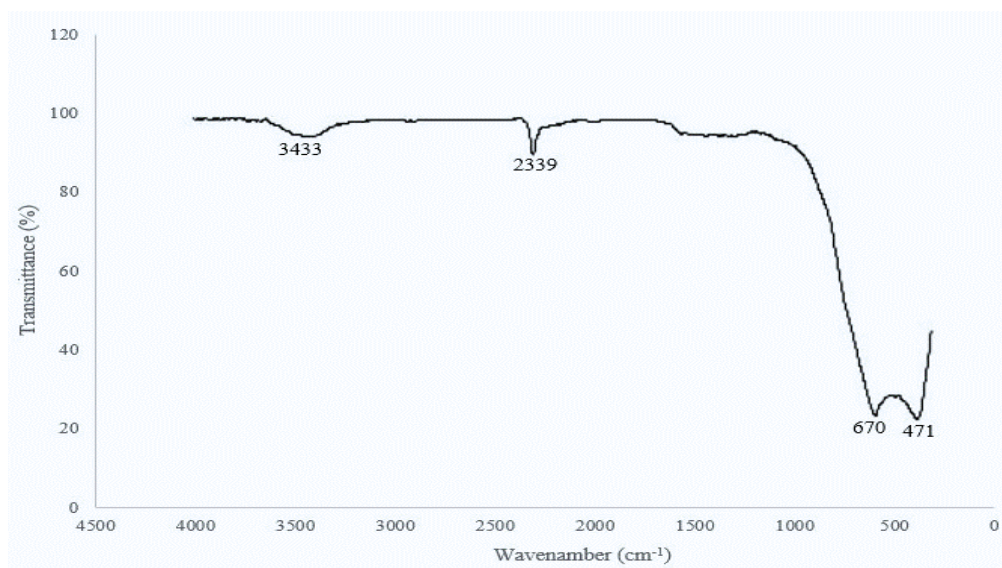
Fig. 6. The FTIR analysis of the synthesized TiO$_2$ nanofibers

increasing humidity from a certain level prevents the formation of nanofibers and instead the titanium dioxide particles are sprayed droplet wise on the aluminum foil.

In the spectra of the calcined TiO$_2$ nanofibers at 500 ºC, and according to the previous studies (e.g. Li and Xia (23) and Dubey et al. (28)) at low frequencies of less than 1000 cm^{-1} are reflects of the stretching vibration of Ti-O-Ti bonds (28, 29). In Fig.6, the FTIR analysis of the TiO$_2$ nanofibers shows two absorption peaks in the regions of 471 cm^{-1} and 670 cm^{-1} which is related to titanium dioxide bond. In Fig.6, in addition to the Ti-O-Ti bond peaks, the peak of O-H was also observed in the reign of 3433 cm^{-1}. The peak appears on 2339 cm^{-1} probably indicates the potential for impurities.

X-Ray Diffraction (XRD) using CuKa radiation (λ= 1.54 A˚) at 40 kV and 30 mA at a size step of 0.040˚ and time step of 1 s (EXPLORER, GNR, Italy) was used to determine the form of amorphous or crystalline nanofibers. In determination of TiO$_2$ nanofiber phases, two phases of the Anatase and Rutile are important. At 200 °C, both polymer and solvents were removed from the nanofibers and the pure titanium dioxide nanofibers were obtained, possessing less diameter. Fig.7 shows the XRD analysis of the nanofibers synthesized with PVP / TiO$_2$ solution at ambient humidity of 37.5% and were then heated at 530 °C.

According to Fig.7a, nanofibers had a pure

Anatase phase and no rutile phase was observed (30). The same analyses were performed for the other nanofibers at different levels of humidity. It should be noted that at temperatures above 600 °C the rutile phase began to form and at 800 °C the pure rutile phase was obtained which is in agreement with the previous studies (31). The peaks at 25.5º, 38.8º, 48.08º, 54.94º, 62.79º, 69.31º, 70.11º and 75.58º which are correspond to the planes of (101), (004), (200), (105), (211), (204), (116), (220) and (215) show the Anatase phase of the TiO$_2$ nanofibers (32). To verify the TiO$_2$ nanofibers, EDX analysis was also performed on the obtained structures (Fig.7 (b)). As seen in its corresponding EDX data from the area analyses of the nanofiber, the presence of Ti from this image clearly corresponds to the occurrence of pristine TiO$_2$ nanofibers.

Fig.8 shows the TEM images of different nanofibers formed from a solution containing 2 mL of titanium isopropoxide, 2 mL of ethanol and 2 mL of acetic acid in titanium solution and 6 mL of ethanol and 0.5 g of polyvinylpyrrolidone in the polymer solution. The nanofibers were calcinated at 500 °C and the effect of ambient relative humidity changing from 24 to 42% was investigated. It is clearly seen the effect of relative humidity on building blocks of the nanofibers. The relative humidity of 24% provided the nanofibers with fairly smooth and porous surface and a larger diameter (Fig.8a). At 28% humidity, it is seen that
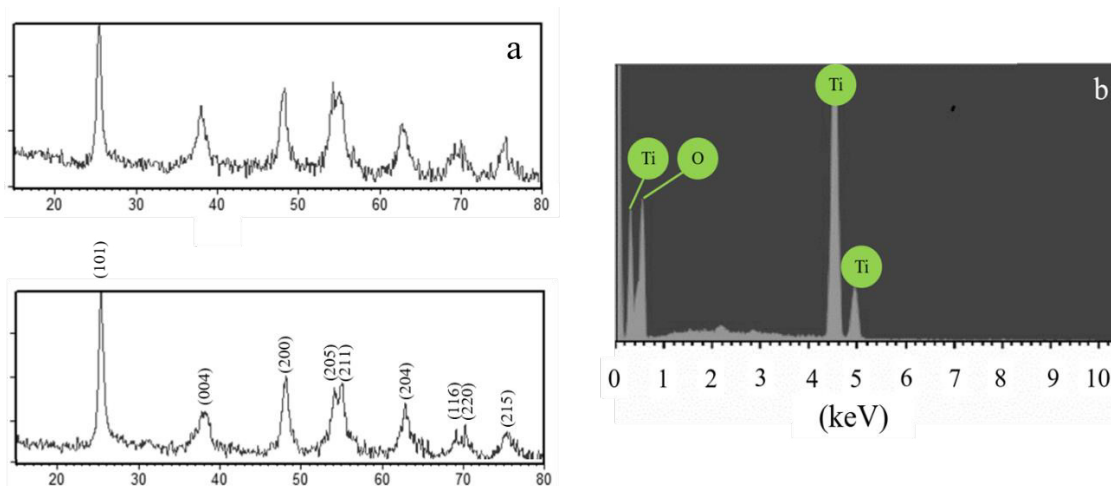
Fig. 7.a) The XRD analysis of the three samples of TiO$_2$ nanofibers heated at 530 °C. b) The EDX area of the TiO$_2$ nanofibers
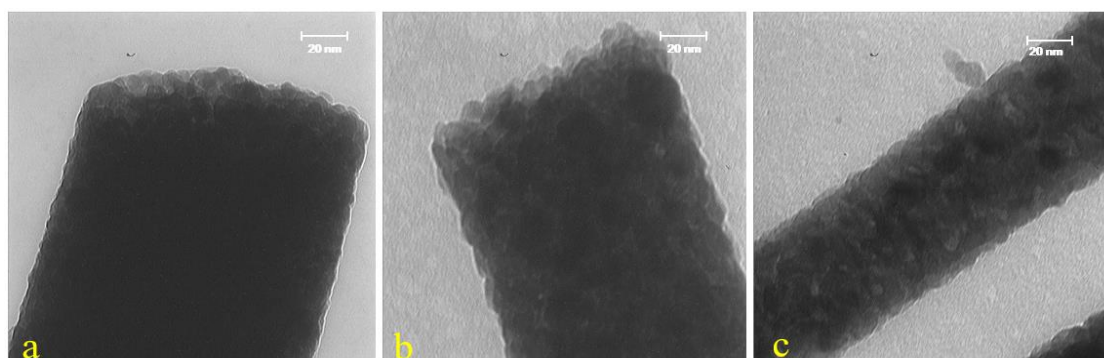

Fig. 8. TEM image of different nanofibers synthesis at different ambient relative humidity
a) 24%. b) 28.5%. c) 37.5%.

porosity increased, while the nanofiber diameter reduced (Fig.8b). This trend is also observed for further increase of relative humidity. The growing rate of porosity and reducing rate of diameter with increase of humidity has continued up to 39%, marking the effect of relative humidity on diameter and morphology of the nanofibers.

The nanofiber does not form higher than the aforementioned percent of relative humidity, which is vividly shown in the SEM image (Fig. 5). Therefore, it can be concluded that having very damp laboratory space, prevents the formation of fibers. Moreover, as illustrated in the TEM images, it is shown that different levels of humidity have a significant effect on the diameter and morphology of electrospun titanium dioxide.

CONCLUSION

Response surface methodology was employed to verify the effect of polymer concentration, distance of needle tip to electrodes, voltage between electrodes, flow rate and relative humidity of the synthesis process on diameter of TiO$_2$ nanofibers with electrospinning method. The quadratic model was chosen as the most efficient model in predicting nanofiber diameter and the polymeric content of nanofibers synthesis solution has the greatest effect on the physical structure of the nanofibers. Some interactions were found to significantly influence the response. Therefore, when synthesizing these nanofibers, the effective factors including polymer content, voltage and ambient humidity should be closely controlled.

According to the results, with increasing the humidity of synthesizer atmosphere to a threshold level (39% in this study), the nanofiber diameter decreases to a minimum and its morphological characteristics are also improved (more porous fibers). However, further investigation should be carried out with varying relative humidity of the synthesizing environment from 35 to 45%, with a smaller increment, to find out a more accurate relative humidity threshold. Corresponding results of this study showed potential ability to produce various diameters for nanofibers in controlled situation.

ACKNOWLEDGMENTS

CONFLICT OF INTEREST

The authors declare that there are no conflicts of interest regarding the publication of this manuscript.

REFERENCES

1. Zhang H, Ye J, Qin X. Facile fabrication and transistor properties of mixed crystalline TiO2 nanofibers FET devices. Materials Letters. 2019;246:99-102.
2. Hosseinpanahi K, Abbaspour-Fard MH, Feizy J, Reza Golzarian M. Dye-Sensitized Solar Cell Using Saffron Petal Extract as a Novel Natural Sensitizer. Journal of Solar Energy Engineering. 2016;139(2).
3. Mansouri S, Abbaspour-Fard MH, Meshkini A. Lily (Iris Persica) pigments as new sensitizer and TiO2 nanofibers as photoanode electrode in dye sensitized solar cells. Optik. 2020;202:163710.
4. Eskandari N, Nabiyouni G, Masoumi S, Ghanbari D. Preparation of a new magnetic and photo-catalyst CoFe2O4–SrTiO3 perovskite nanocomposite for photo-degradation of toxic dyes under short time visible irradiation. Composites Part B: Engineering. 2019;176:107343.
5. Kiani A, Nabiyouni G, Masoumi S, Ghanbari D. A novel magnetic MgFe2O4–MgTiO3 perovskite nanocomposite: Rapid photo-degradation of toxic dyes under visible irradiation. Composites Part B: Engineering. 2019;175:107080.
6. Ahmadian-Fard-Fini S, Ghanbari D, Amiri O, Salavati-Niasari M. Electro-spinning of cellulose acetate nanofibers/Fe/carbon dot as photoluminescence sensor for mercury (II) and lead (II) ions. Carbohydrate Polymers. 2020;229:115428.
7. Bagheri A, Halakouie H, Ghanbari D, Mousayi M, Asiabani N. Strontium hexa-ferrites and polyaniline nanocomposite: Studies of magnetization, coercivity, morphology and microwave absorption. J Nanostructu. 2019;9(4):630-638.
8. Namvar MJ, Abbaspour-Fard MH, Rezaee Roknabadi M,

Behjat A, Mirzaei M. Enhancement of perovskite solar cells characteristics by incorporating mixed sodium/cesium cations. Optik. 2019;185:1019-23.
9. Sorinezami Z, Ghanbari D. Facile preparation of silver nanoparticles and antibacterial Chitosan-Ag polymeric nanocomposites. J Nanostruct. 2019;9(3):396-401.
10. Katoch A, Choi S-W, Kim SS. Nanograins in electrospun oxide nanofibers. Metals and Materials International. 2015;21(2):213-21.
11. Yavari M, Mazloum-Ardakani M, Khoshroo A. Core–shell titanium dioxide/carbon nanofibers decorated nickel nanoparticles as supports for electrocatalytic oxidation of ethanol. J Nanostruct. 2019;9(2):268-275.
12. Aghasiloo P, Yousefzadeh M, Latifi M, Jose R. Highly porous TiO2 nanofibers by humid-electrospinning with enhanced photocatalytic properties. Journal of Alloys and Compounds. 2019;790:257-65.
13. Cui L, Liu S, Wang F, Li J, Song Y, Sheng Y, et al. Growth of uniform g-C3N4 shells on 1D TiO2 nanofibers via vapor deposition approach with enhanced visible light photocatalytic activity. Journal of Alloys and Compounds. 2020;826:154001.
14. Ma C, Wei M. BiVO4-nanorod-decorated rutile/anatase TiO2 nanofibers with enhanced photoelectrochemical performance. Materials Letters. 2020;259:126849.
15. Narayan MR. Review: Dye sensitized solar cells based on natural photosensitizers. Renewable and Sustainable Energy Reviews. 2011.
16. Choi SK, Kim S, Lim SK, Park H. Photocatalytic Comparison of TiO2Nanoparticles and Electrospun TiO2Nanofibers: Effects of Mesoporosity and Interparticle Charge Transfer. The Journal of Physical Chemistry C. 2010;114(39):16475-80.
17. Mehdizadeh P. Photocatalyst Ag@N/TiO2 Nanoparticles: Fabrication, Characterization, and Investigation of the Effect of Coating on Methyl Orange Dye Degradation. Journal of Nanostructures. 2017;7(3).
18. Mali SS, Shim CS, Kim H, Patil JV, Ahn DH, Patil PS, et al. Evaluation of various diameters of titanium oxide nanofibers for efficient dye sensitized solar cells synthesized by electrospinning technique: A systematic study and their application. Electrochimica Acta. 2015;166:356-66.
19. Minchi L, Cao F, Xinni Z, Youqiang C, Xuhua L. Photocatalytic activity of Ca-TiO2 nanofibers with different concentrations of calcium. Chemical Physics Letters. 2019;736:136807.
20. Thoppey NM, Bochinski JR, Clarke LI, Gorga RE. Edge electrospinning for high throughput production of quality nanofibers. Nanotechnology. 2011;22(34):345301.
21. Pai C-L, Boyce MC, Rutledge GC. Morphology of Porous and Wrinkled Fibers of Polystyrene Electrospun from Dimethylformamide. Macromolecules. 2009;42(6):2102-14.
22. Şimşek M. Tuning surface texture of electrospun polycaprolactone fibers: Effects of solvent systems and relative humidity. Journal of Materials Research. 2020;35(3):332-42.
23. Li D, Xia Y. Fabrication of Titania Nanofibers by Electrospinning. Nano Letters. 2003;3(4):555-60.
24. Sarlak N, Nejad MAF, Shakhesi S, Shabani K. Effects of electrospinning parameters on titanium dioxide nanofibers diameter and morphology: An investigation by Box–Wilson central composite design (CCD). Chemical Engineering Journal. 2012;210:410-6.

25. Sreethawong T, Laehsalee S, Chavadej S. Comparative investigation of mesoporous- and non-mesoporous-assembled TiO2 nanocrystals for photocatalytic H2 production over N-doped TiO2 under visible light irradiation. International Journal of Hydrogen Energy. 2008;33(21):5947-57.

26. Joudaki H, Mousavi M, Safari M, Razavi SH, Emam-Djomeh Z, Gharibzahedi SMT. A practical optimization on salt/high-methoxyl pectin interaction to design a stable formulation for Doogh. Carbohydrate Polymers. 2013;97(2):376-83.

27. Park JY, Kim SS. Effects of processing parameters on the synthesis of TiO2 nanofibers by electrospinning. Metals and Materials International. 2009;15(1):95-9.

28. Dubey PK, Tripathi P, Tiwari RS, Sinha ASK, Srivastava ON. Synthesis of reduced graphene oxide–TiO 2 nanoparticle composite systems and its application in hydrogen

29. production. International Journal of Hydrogen Energy. 2014;39(29):16282-92.

29. Li H, Cui X. A hydrothermal route for constructing reduced graphene oxide/TiO2 nanocomposites: Enhanced photocatalytic activity for hydrogen evolution. International Journal of Hydrogen Energy. 2014;39(35):19877-86.

30. Nabiyouni G, Ghanbari D. Simple preparation of magnetic, antibacterial and photo-catalyst NiFe$_2$O$_4$@ TiO$_2$/Pt nanocomposites. J Nanostruct. 2018;8(4):408-416.

31. Caratão B, Carneiro E, Sá P, Almeida B, Carvalho S. Properties of Electrospun TiO2Nanofibers. Journal of Nanotechnology. 2014;2014:1-5.

32. Xing X, Chen N, Yang Y, Zhao R, Wang Z, Wang Z, et al. Pt-Functionalized Nanoporous TiO2 Nanoparticles With Enhanced Gas Sensing Performances Toward Acetone. physica status solidi (a). 2018;215(14):1800100.